ADVANCED FUNCTIONAL MATERIALS
www.afm-journal.de

Materials Views
www.MaterialsViews.com

Ultrathin Mesoporous $NiCo_2O_4$ Nanosheets Supported on Ni Foam as Advanced Electrodes for Supercapacitors

*Changzhou Yuan, Jiaoyang Li, Linrui Hou, Xiaogang Zhang, Laifa Shen, and Xiong Wen (David) Lou**

A facile two-step method is developed for large-scale growth of ultrathin mesoporous nickel cobaltite ($NiCo_2O_4$) nanosheets on conductive nickel foam with robust adhesion as a high-performance electrode for electrochemical capacitors. The synthesis involves the co-electrodeposition of a bimetallic (Ni, Co) hydroxide precursor on a Ni foam support and subsequent thermal transformation to spinel mesoporous $NiCo_2O_4$. The as-prepared ultrathin $NiCo_2O_4$ nanosheets with the thickness of a few nanometers possess many interparticle mesopores with a size range from 2 to 5 nm. The nickel foam supported ultrathin mesoporous $NiCo_2O_4$ nanosheets promise fast electron and ion transport, large electroactive surface area, and excellent structural stability. As a result, superior pseudocapacitive performance is achieved with an ultrahigh specific capacitance of 1450 F g^{-1}, even at a very high current density of 20 A g^{-1}, and excellent cycling performance at high rates, suggesting its promising application as an efficient electrode for electrochemical capacitors.

1. Introduction

In recent years, electrochemical capacitors (ECs), also called supercapacitors, have attracted tremendous interest as power sources for applications requiring quick bursts of energy, such as high power electronic devices and electric vehicles. ECs are able to deliver higher power density with better cycling lifespan over batteries, and store more energy than conventional capacitors. ECs commonly store energy based on either ion adsorption (electrochemical double layer capacitors, EDLCs) or fast surface redox reactions (pseudocapacitors).[1,2] Unfortunately, the low specific capacitance (SC) of EDLCs cannot meet the ever-growing need for peak-power assistance in electric vehicles, and so on. Thus, growing interest in using pseudocapacitive materials for ECs has been triggered because the energy density associated with Faradaic reactions is substantially larger by at least one order of magnitude than that of EDLCs.[3–5] In common, pseudocapacitive materials, which mainly include metal hydroxides, oxides and conductive polymers, possess multiple oxidation states/structures that are capable of rich redox reactions. One of the most notable pseudocapacitive materials studied is RuO_2. However, its large-scale application is hindered by the very high cost and rareness of the Ru element.[6,7] Among many metal oxides, spinel nickel cobaltite ($NiCo_2O_4$) has been conceived as a promising cost-effective and scalable alternative since it offers many advantages such as low cost, abundant resources and environmental friendliness.[4,8–12] More importantly, it is reported that spinel $NiCo_2O_4$ possesses much better electrical conductivity, at least two orders of magnitude higher, and higher electrochemical activity than nickel oxides or cobalt oxides.[13,14] It is therefore expected to offer richer redox reactions, including contributions from both nickel and cobalt ions, than those of the monometallic nickel oxides and cobalt oxide.[4,8–12] These attractive features are of great advantage for its application in high-performance ECs.

To maximize the electrochemical performance of a pseudocapacitor, one needs to engineer the electrodes with large amount of electroactive sites and high transport rates for both electrolyte ions and electrons that simultaneously take part in the Faradaic reactions.[5] More specifically, the former requires large specific surface area (SSA) of electroactive materials, which will promote the electric double-layer capacitance and accommodate a large amount of superficial electroactive species for participation in the Faradaic redox reactions. While the later entails fast diffusion of the electrolyte ions and fast conduction of electrons to the electroactive sites. This can be achieved by concocting mesoporous porosity into the electroactive materials with large naked SSA, high electrical conductivity and fast ion transport.

However, $NiCo_2O_4$-based electrodes are commonly binder-enriched electrodes made by the traditional slurry-coating technique for electrochemical evaluation,[4,8–12] where a large portion of the electroactive $NiCo_2O_4$ surface is "dead surface" and blocked from the contact with the electrolyte to participate

Dr. C. Z. Yuan, J. Y. Li, L. R. Hou
Anhui Key Laboratory of Metal Materials and Processing
School of materials Science and Engineering
Anhui University of technology
Màanshan, 243002, P. R. China
Dr. C. Z. Yuan, Prof. X. W. Lou
School of Chemical and Biomedical Engineering
Nanyang Technological University
70 Nanyang Drive, Singapore 637457
E-mail: xwlou@ntu.edu.sg
Prof. X. G. Zhang, L. F. Shen
College of Material Science & Engineering
Nanjing University of Aeronautics and Astronautics
Nanjing, 210016, P. R. China

DOI: 10.1002/adfm.201200994

in the Faradaic reactions for energy storage. Moreover, the binder involved will greatly decrease the electrical conductivity of the electrode materials, hindering their potential application in high-performance ECs.[15–17] As an example, Hu et al. synthesized spinel $NiCo_2O_4$ nanoparticles (NPs) by a sol-gel process, and these NPs exhibit ultrahigh SC of 1400 F g^{-1} (the loading of $NiCo_2O_4$ is 0.4 mg cm^{-2}) after a 650-cycle activation process.[9] Unfortunately, the high rate performance is still unsatisfactory. Therefore, to achieve even better electrochemical performance, it is highly desirable to directly disperse and wire up electroactive mesoporous $NiCo_2O_4$, particularly with desirable mesoporosity of 2–5 nm,[18–20] to an underlying conductive substrate. By this way, the conventional tedious process of electrode making can be avoided, and more importantly, electroactive $NiCo_2O_4$ with large naked surface and good electrical conductivity can be placed in direct contact with both the electrolyte and the substrate for efficient energy storage at high rates.

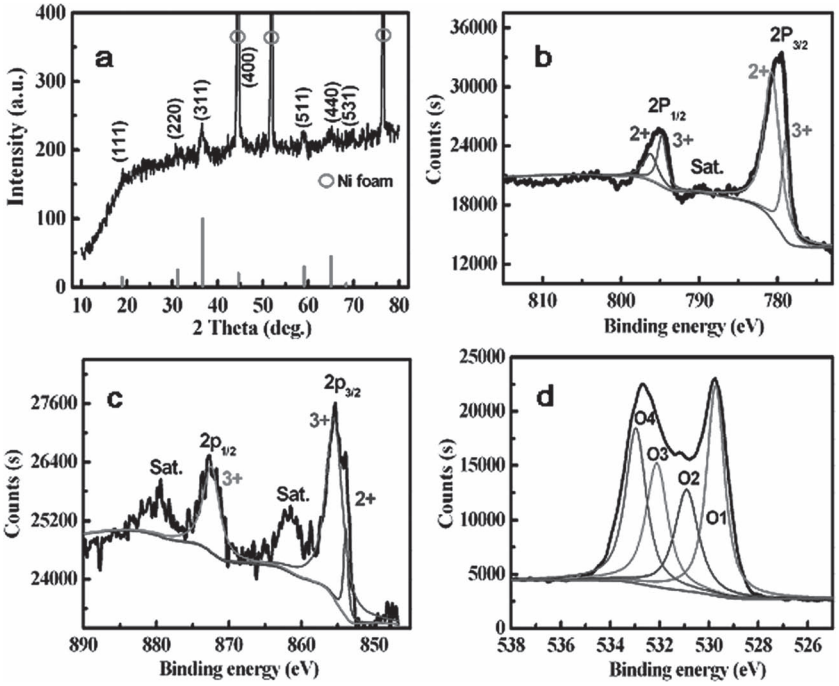

Figure 1. a) XRD pattern of the $NiCo_2O_4$ nanosheets/Ni foam. High-resolution XPS spectra of b) Co 2p, c) Ni 2p, and d) O 1s for the ultrathin mesoporous $NiCo_2O_4$ nanosheets scratched down from the Ni foam.

Based on the above considerations, we develop a facile two-step strategy to grow ultrathin mesoporous $NiCo_2O_4$ nanosheets on nickel foam with robust adhesion and the hybrid structure is then directly used as an electrode for electrochemical evaluation in a three-electrode system at room temperature. The synthesis involves the co-electrodeposition of the bimetallic (Ni, Co) hydroxide precursor on Ni foam support and subsequent thermal transformation to ultrathin mesoporous spinel $NiCo_2O_4$ nanosheets in the absence of any templates. Remarkably, the as-prepared 3D hybrid structure of nickel foam supported ultrathin mesoporous $NiCo_2O_4$ nanosheets manifests ultrahigh SCs and good cycling stability at high rates in a 3 M KOH aqueous electrolyte, making it a promising electrode for ECs.

2. Results and Discussion

2.1. Synthesis and Structural Analysis

In our synthesis strategy, two steps are involved: co-electrodeposition of mixed metal (Ni, Co) hydroxide precursor followed by a calcination process in air. Firstly, a green bimetallic (Ni, Co) hydroxide precursor is co-electrodeposited onto the Ni foam, which is nearly amorphous (Figure S1, see Supporting Information). When the electric current passes through the electrolyte containing Ni^{2+} and Co^{2+} with a molar ratio of 1: 2, NO_3^- can be reduced on the cathodic surface to produce hydroxide ions. The generation of OH^- ions at the cathode raises the local pH value, resulting in the uniform precipitation of mixed (Ni, Co) hydroxide on the Ni foam surface considering that the solubility product constant (K_{sp}) at 25°C of $Co(OH)_2$ (2.5×10^{-16}) is very close to that of $Ni(OH)_2$ (2.8×10^{-16}).[4] The whole process may comprise an electrochemical reaction and subsequent precipitation of mixed hydroxide (donated as $M(OH)_2$ (M = Co^{2+} and Ni^{2+}), where the molar ratio of Co^{2+} and Ni^{2+} is 2: 1), as described by the following two equations:

$$NO_3^- + 7H_2O + 8e^- \rightarrow NH4^+ + 10\,OH^- \quad (1)$$

$$x\,Ni^{2+} + 2x\,Co^{2+} + 6x\,OH^- \rightarrow Ni_xCo_{2x}\,(OH)_{6x} \quad (2)$$

Then, the formed hydroxides are thermally transformed to black spinel $NiCo_2O_4$ supported on the Ni foam, as described by the simple oxidation reaction as follows:

$$Ni_xCo_{2x}\,(OH)_{6x} + \frac{1}{2}x\,O_2 \rightarrow x\,NiCo_2O_4 + 3x\,H_2O \quad (3)$$

Figure 1a shows the wide-angle X-ray diffraction (XRD) pattern of the ultrathin mesoporous $NiCo_2O_4$ nanosheets supported on Ni foam. As observed in Figure 1a, except for the three typical peaks originating from the Ni substrate, other seven well-defined diffraction peaks are observed at 2θ values of 18.9°, 31.1°, 36.6°, 44.6°, 59.1°, 64.9° and 68.3°. All of these peaks can be successfully indexed to (111), (220), (311), (400), (511), (440) and (531) plane reflections of the spinel $NiCo_2O_4$ crystalline structure (JCPDF file no. 20-0781; space group: *F*3* (202)), with the standard peaks indicated by the red lines in Figure 1a. Moreover, the diffraction intensities of Ni foam are dramatically diminished after being covered by the $NiCo_2O_4$ (Figure S2, Supporting Information), suggesting that the $NiCo_2O_4$ is uniformly grown upon the Ni foam surface.

The more detailed elemental composition and the oxidation state of the as-prepared $NiCo_2O_4$ are further characterized by

X-ray photoelectron (XPS) measurements and the corresponding results are presented in Figure 1b–d. By using a Gaussian fitting method, the Co 2p emission spectrum (Figure 1b) was best fitted with two spin-orbit doublets, characteristic of Co^{2+} and Co^{3+}, and one shakeup satellite (indicated as "Sat."). [21] The Ni 2p was also fitted with two spin-orbit doublets, characteristic of Ni^{2+} and Ni^{3+}, and two shakeup satellites. The high-resolution spectrum for the O 1s region (Figure 1d) shows four oxygen contributions, which have been denoted as O1, O2, O3, and O4, respectively. Specifically, the component O1 at 529.2 eV is typical of metal-oxygen bonds. [22,23] The component O2 sitting at 530 eV is usually associated with oxygen in OH^- groups and the presence of this contribution in the O 1s spectrum indicates that the surface of the $NiCo_2O_4$ material is hydroxylated to some extent as a result of either surface oxydroxide or the substitution of oxygen atoms at the surface by hydroxyl groups. [24] The well-resolved O3 component corresponds to a higher number of defect sites with low oxygen coordination usually observed in materials with small particles. [25] The component O4 can be attributed to multiplicity of physi- and chemi-sorbed water at or near the surface. [23,26] These data show that the surface of the as-prepared $NiCo_2O_4$ has a composition containing Co^{2+}, Co^{3+}, Ni^{2+}, and Ni^{3+}. Thus, the formula of $NiCo_2O_4$ can be generally expressed as follows: $Co^{2+}_{1-x}Co^{3+}_x[Co^{3+}Ni^{2+}_xNi^{3+}_{1-x}]O_4$ ($0 < x < 1$) (the cations within the square bracket are in octahedral sites and the outside ones occupy the tetrahedral sites), [27,28] where the atomic ratio of Co to Ni elements is ca. 2.1: 0.9, close to that in the precursor electrolyte.

Figure 2a shows a representative low-magnification field-emission scanning electron microscopy (FESEM) image of the bimetallic (Ni, Co) hydroxide precursor supported on the nickel foam substrate. Clearly, a 3D grid structure with hierarchical macro-porosity can still be found as that in the pristine Ni foam. To further reveal its microstructure, Figure 2b shows a high-magnification top-view FESEM image of the region marked by the rectangle in Figure 2a. Evidently, the (Ni, Co) hydroxide precursor possesses a nanosheet micro-structure with rippled silk morphology due to its ultrathin feature. And after oxidative conversion into spinel $NiCo_2O_4$, the basic morphology of the sample is perfectly conserved without calcination-induced significant alterations (Figure 2c,d). These as-formed nanosheets with a lateral size of several hundred nanometers are intercrossed with each other, which creates loose porous nanostructures with abundant open space and electroactive surface sites.

Transmission electron microscopy (TEM) measurements were carried out to further investigate the structure of the as-synthesized $NiCo_2O_4$ nanosheets. As can be seen from **Figure 3**a,b, the $NiCo_2O_4$ nanosheets exhibit folding silk-like morphology with transparent feature, indicating the ultrathin nature. Due to the much larger lateral size than the thickness, the morphologies of bending, curling, and crumpling are clearly observed. The dark strips are generally the folded edges or wrinkles of the nanosheets. It reveals that the nanosheets are only 2–4 nm in thickness. The number of lattice layers constituting the nanosheets can be determined from the curling folded edges, as seen from the high-resolution TEM image (Figure 3c) of the region marked by a rectangle in Figure 3b. The spacing between adjacent fringes is *ca.* 0.47 nm, close to the theoretical interplane spacing of spinel $NiCo_2O_4$ (111) planes. Thus, the ultrathin nanosheets should be composed of 3–6 layers of $NiCo_2O_4$ atomic sheets. The selected-area electron diffraction (SAED) pattern (Figure 3d) shows well-defined diffraction rings, suggesting their polycrystalline characteristics. Moreover, numerous inter-particle mesopores with a size ranged from 2 to 5 nm in these ultrathin nanosheets can be clearly seen (Figure 3a,b), which results from the thermal decomposition of the hydroxides. It is well known that the mesoporous structures in nanosheets are important to facilitate the mass transport of electrolytes within the electrodes for fast redox reactions and double-layer charging/discharging. The porous structure will also greatly increase the electrode/electrolyte contact area, and thus further enhance the electrochemical performance. To highlight the merits of the unique architecture, we directly apply the hybrid structure of ultrathin mesoporous $NiCo_2O_4$ nanosheets supported on Ni foam as an electrode for ECs.

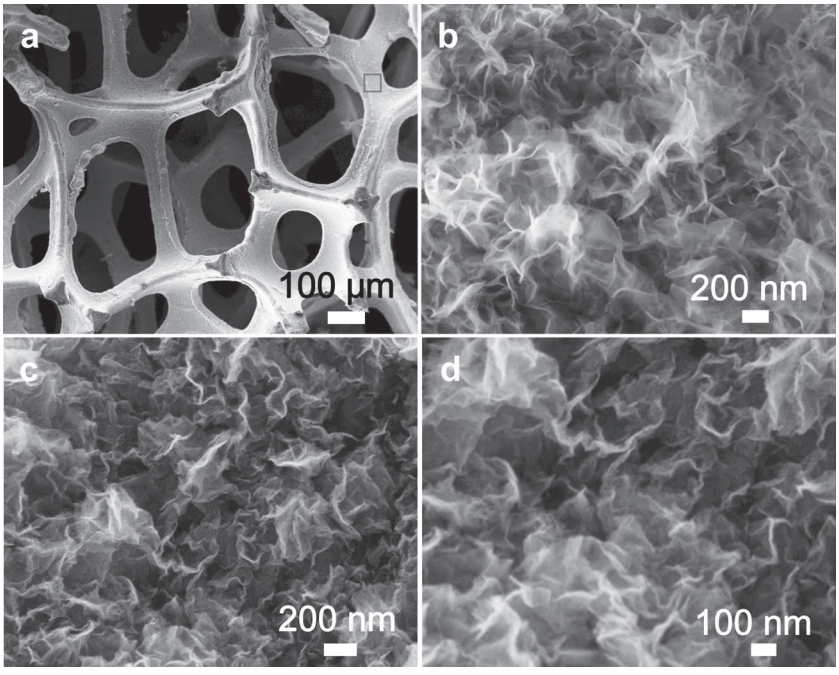

Figure 2. FESEM images of Ni foam covered by the bimetallic (Ni, Co) hydroxide precursor (a,b) and the derived $NiCo_2O_4$ utrathin nanosheets/Ni foam (c,d). The image in (b) is taken from the region marked with a rectangle in (a).

2.2. Electrochemical Evaluation

Cyclic voltammetry (CV) and chronopotentiometry (CP) measurements were conducted in a three-electrode cell to evaluate the electrochemical properties of the ultrathin mesoporous $NiCo_2O_4$ nanosheets supported on Ni foam. **Figure 4**a shows the representative CV curves of the self-supported $NiCo_2O_4$ nanosheets electrode in a 3 M KOH aqueous electrolyte at various scan rates ranged from

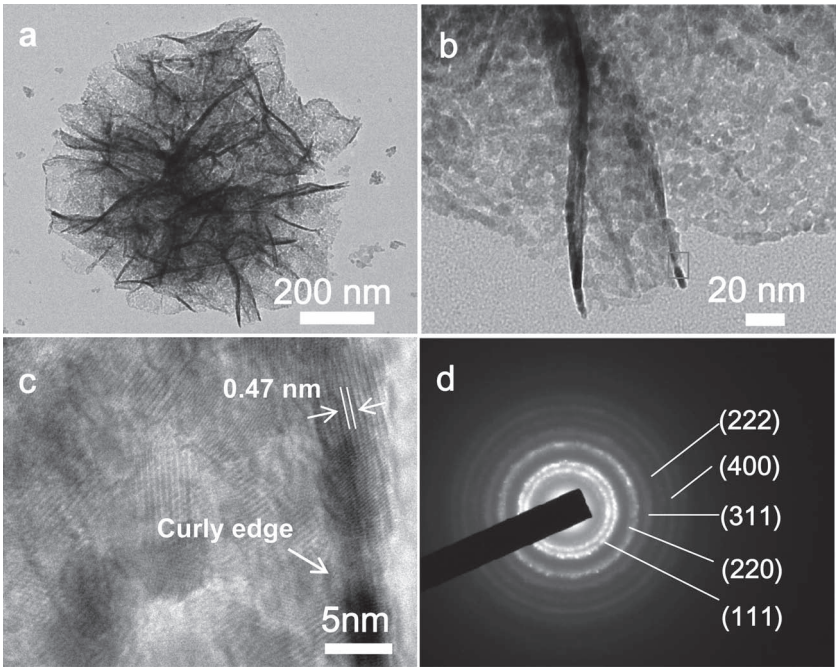

Figure 3. a,b) TEM, c) HRTEM images, and d) SAED pattern of the ultrathin mesoporous $NiCo_2O_4$ nanosheets scratched down from the Ni foam. The image in (c) is taken from the region marked with a rectangle in (b).

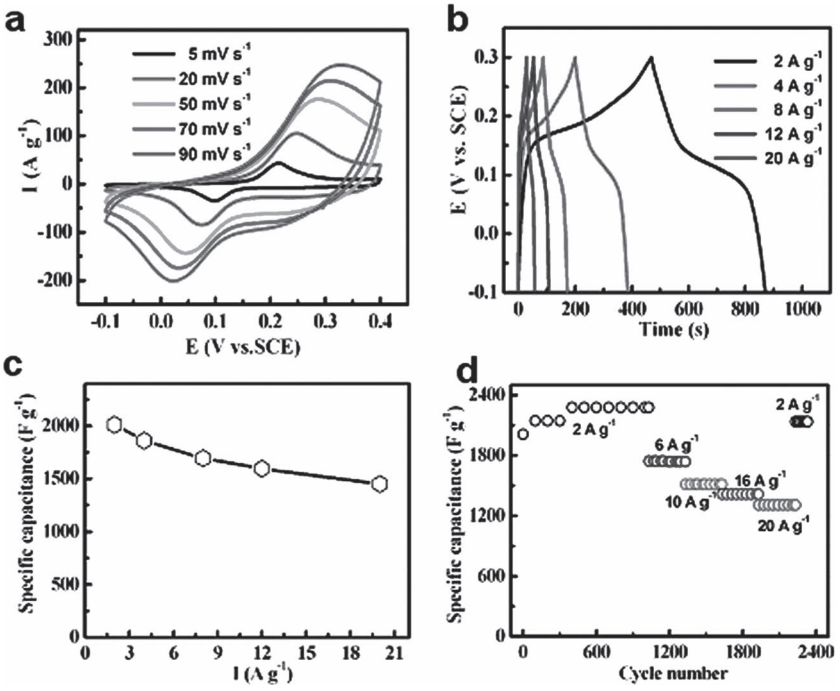

Figure 4. Electrochemical evaluations of Ni foam-supported ultrathin mesoporous $NiCo_2O_4$ nanosheets: a) CV curves, b) constant-current charge-discharge voltage profiles, c) the corresponding specific capacitance as a function of current density, and d) cycling performance at progressively varying current densities.

5 to 90 mV s^{-1}. Clearly, a pair of well-defined redox peaks within –0.1–0.4 V (vs. SCE) is visible in all CV curves. This indicates that the electrochemical capacitance of the ultrathin mesoporous $NiCo_2O_4$ nanosheets electrode is distinct from electric double-layer capacitance characterized by nearly rectangular CV curves. And this pair of peaks is mainly attributed to the Faradaic redox reactions related to M-O/M-O-OH (M represents Ni or Co).[8] The high-power characteristic of the unique electrode can be identified from their voltammetric response at various scan rates. Apparently, all curves exhibit a similar shape, and the current density increases with the increasing scan rate. Even at a scan rate of 90 mV s^{-1}, the CV curve still shows a pair of redox peaks, indicating that this hybrid structure is beneficial to fast redox reactions. Remarkably, the peak potential shifts only *ca.* 100 mV for an 18-time increase in the scan rate, suggesting that the electrode possesses low polarization. This is expected because the Ni foam support will ensure excellent electric conductivity of the hybrid structure electrode,[3,29] which can be further verified by the electrochemical impedance spectroscopy (EIS; see Supporting Information, Figure S4) measurement. Furthermore, a linear relation between the oxidation peak current at different scan rates and the square root of the scan rate is observed (Figure S3, Supporting Information), confirming that the redox reaction is a diffusion-controlled process.

To further evaluate the application potential of the as-synthesized hybrid structure as an electrodes for ECs, galvanostatic charge-discharge measurements were carried out in a 3 M KOH electrolyte between –0.1 and 0.3 V (vs. SCE) at various current densities ranging from 2 to 20 A g^{-1}, as shown in Figure 4b. The observation of nearly symmetric potential-time curves at all current densities implies the high charge-discharge coulombic efficiency and low polarization of the unique electrode. The SCs of the $NiCo_2O_4$ ultrathin nanosheets electrode can be calculated based on the charge-discharge curves in Figure 4b and the results are plotted in Figure 4c. Encouragingly, the Ni foam-supported ultrathin mesoporous $NiCo_2O_4$ nanosheets electrode exhibits excellent pseudocapacitance of 2010, 1859, 1694, 1596 and 1450 F g^{-1} at current densities of 2, 4, 8, 12 and 20 A g^{-1}, respectively. This suggests that about 72% of the capacitance is still retained when the charge-discharge rate is increased from 2 to 20 A g^{-1}. To the best of our knowledge, such superior pseudocapacitive

performance is rarely observed for electroactive $NiCo_2O_4$,[4,8–12] which might be attributed to the advantageous structure of the present electrode. Specifically, the ultrathin and mesoporous characteristics of the nanosheets give rise to very high surface area, providing numerous electroactive sites for redox reaction. Moreover, the open space between these ultrathin nanosheets and the mesopores existing in the nanosheets can sever as a robust reservoir for ions, and also greatly enhance the diffusion kinetics within the electrode. In other words, these hierarchical porous channels ensure efficient contact between the surface of electroactive nanosheets and the electrolyte even at high rates. Furthermore, the direct contact of each nanosheet with good intrinsic electrical conductivity to the underneath conductive Ni foam substrate builds up an express path for fast electron transport, thus avoiding the use of polymer binder and conductive additive which commonly add extra contact resistance.

The long-term cycling performance of this hybrid electrode at progressively increasing current densities is recorded as shown in Figure 4d. It can be observed that the SC increases gradually up to 2278 F g^{-1} in the course of initial 400 cycles instead of decreasing as in most cycling stability tests in the literature, which can be attributed to the full activation of the present electrode. Importantly, the Ni foam-supported $NiCo_2O_4$ nanosheets electrode exhibits stable cycling performance at each current density. After continuous cycling for 2300 cycles at various current densities, the current density is reduced back to 2 A g^{-1}. Remarkably, ca. 94% of the initial capacitance at 2 A g^{-1} can still be delivered and maintained for another 100 cycles without noticeable diminishment. Based on the above overall electrochemical performance, the unique ultrathin mesoporous $NiCo_2O_4$ nanosheets/Ni foam electrode is apparently superior to many other $NiCo_2O_4$ electrodes, as can be seen from the Table S1 (Supporting Information). These results evidently suggest the great promise of this hybrid Ni foam supported $NiCo_2O_4$ nanosheets electrode for high-performance ECs characterized by both long cycle life and excellent rate capability.

3. Conclusions

In summary, we have fabricated an advanced three-dimensional electrode by growing ultrathin mesoporous $NiCo_2O_4$ nanosheets on Ni foam with strong adhesion for high-performance electrochemical capacitors. The efficient two-step synthesis involves a co-electrodeposition of bimetallic (Ni, Co) hydroxide precursor on Ni foam, and subsequent thermal conversion into spinel $NiCo_2O_4$. The as-obtained $NiCo_2O_4$ ultrathin nanosheets possess numerous inter-particle mesopores with a size of 2 to 5 nm. Owing to these advantageous structural features, this self-supported hybrid electrode of ultrathin mesoporous $NiCo_2O_4$ nanosheets supported on Ni foam is able to deliver ultrahigh specific capacitance of 2010 and 1450 F g^{-1} at current densities of 2 and 20 A g^{-1}, respectively, with excellent cycling stability. Our work opens up the possibility of constructing advanced electrodes with high specific capacitance, excellent rate capability and cycling stability for high-performance electrochemical capacitors. More importantly, the electrode design concept can be easily generalized to other binary or ternary metal oxides with unique nano- and microstructures for a large spectrum of device applications.

4. Experimental Section

Synthesis of Ni Foam Supported Ultrathin Mesoporous $NiCo_2O_4$ Nanosheets: All the chemicals were of analytical grade and were used without further purification. Nickel foam (approximately 1 cm × 4 cm) was carefully cleaned with 6 M HCl solution in an ultrasound bath for 30 min in order to remove the NiO layer on the surface, and then rinsed with de-ionized water and absolute ethanol. The electrodeposition was performed in a standard three-electrode glass cell consisting of the clean Ni foam working electrode, a platinum plate counter electrode and a saturated calomel reference electrode (SCE) at a temperature of 10 ± 1 °C. The bimetallic (Ni, Co) hydroxide precursor was electrodeposited upon Ni foam in a 4 mM $Co(NO_3)_2{\cdot}6H_2O$ and 2 mM $Ni(NO_3)_2{\cdot}6H_2O$ aqueous mixed electrolyte using an IVIUM Electrochemical Workstation (the Netherlands). The electrodeposition potential is –1.0 V (vs. SCE). After electrodeposition for 5 min, the green Ni foam was carefully rinsed several times with de-ionized water and absolute ethanol with the assistance of ultrasonication, and finally dried in air. Then, the sample was put in a quartz tube and calcined at 300 °C for 2 h with a ramping rate of 1 °C min^{-1} to transform into ultrathin mesoporous $NiCo_2O_4$ nanosheets. In average, 0.8 mg of $NiCo_2O_4$ nanosheets is grown per 1 cm × 1 cm of Ni foam, carefully weighted after calcination.

Materials Characterization: The samples were characterized by powder X-ray diffraction (XRD) (Max 18 XCE, Japan) using a Cu Kα source (λ = 0.15406 nm) at a scanning speed of 3° min^{-1} over a 2θ range of 10–80°. The morphology was examined with field-emission scanning electron microscope (FESEM; JEOL-6300F, 15 kV) and transmission electron microscope (TEM) capable of high-resolution transmission electron microscope (HRTEM) study and selected area electron diffraction (SAED) (JEOL JEM 2100 system operating at 200 kV). X-ray photoelectron spectroscope (XPS) measurements were performed on a VGESCALAB MKII X-ray photoelectron spectrometer with a Mg Kα excitation source (1253.6 eV).

Electrochemical Tests: The Ni foam-supported ultrathin mesoporous $NiCo_2O_4$ nanosheets directly acted as the working electrode for the following electrochemical tests by cyclic voltammetry (CV), chronopotentiometry (CP) and electrochemical impedance spectroscopy (EIS) performed with a IVIUM electrochemical workstation (the Netherlands). EIS tests were carried out with a frequency loop from 10^5 Hz to 0.01 Hz using perturbation amplitude of 5 mV at 0.2 V versus SCE. All measurements were carried out in a three-electrode cell with a working electrode, a platinum plate counter electrode and a saturated calomel electrode (SCE) as the reference electrode at room temperature. The electrolyte was a 3 M KOH aqueous solution. The cycling performance test was carried out with a CT2001A tester (Wuhan, China).

The specific capacitance (SC) of the self-supported $NiCo_2O_4$ nanosheets electrode is calculated from the CP curves based on the following equation:

$$C = \frac{It}{\Delta V} \tag{4}$$

where C, I, t and ΔV are the SC (F g^{-1}) of the electrodes, the discharging current density (A g^{-1}), the discharging time (s) and the discharging potential range (V), respectively.

Supporting Information

Supporting Information is available from the Wiley Online Library or from the author.

Received: April 8, 2012
Revised: May 21, 2012
Published online: June 26, 2012

[1] B. E. Conway, *Electrochemical Supercapacitors: Scientific Fundamentals and Technological Applications*, Kluwer Academic/Plenum Publishers, New York **1999**.
[2] P. Simon, Y. Gogotsi, *Nat. Mater.* **2008**, *7*, 845.
[3] T. Brezesinski, J. Wang, S. H. Tolbert, B. Dunn, *Nat. Mater.* **2010**, *9*, 146.
[4] J. W. Xiao, S. H. Yang, *RSC Adv.* **2011**, *1*, 588.
[5] C. Z. Yuan, B. Gao, L. F. Shen, S. D. Yang, L. Hao, X. J. Lu, F. Zhang, L. J. Zhang, X. G. Zhang, *Nanoscale* **2011**, *3*, 529.
[6] C. Z. Yuan, L. Chen, B. Gao, L. H. Su, X. G. Zhang, *J. Mater. Chem.* **2009**, *19*, 246.
[7] W. Sugimoto, H. Iwata, Y. Yasunaga, Y. Murakami, Y. Takasu, *Angew. Chem. Int. Ed.* **2003**, *42*, 4092.
[8] H. L. Wang, Q. M. Gao, L. Jiang, *Small* **2011**, *7*, 2454.
[9] T. Y. Wei, C. H. Chen, H. C. Chien, S. Y. Lu, C. C. Hu, *Adv. Mater.* **2009**, *21*, 1.
[10] H. X. Wang, Z. A. Hu, Y. Q. Chang, Y. L. Chen, H. Y. Wu, Z. Y. Zhang, Y. Y. Yang, *J. Mater. Chem.* **2011**, *21*, 10504.
[11] A. C. Tavares, M. A. M. Cartaxo, M. I. da Silva Pereira, F. M. Costa, *J. Solid State Electrochem.* **2001**, *5*, 57.
[12] H. Jiang, J. Man, C. Z. Li, *Chem. Commun.* **2012**, *48*, 4465.
[13] J. P. Liu, Y. Y. Li, X. T. Huang, G. Y. Li, Z. K. Li, *Adv. Funct. Mater.* **2008**, *18*, 1448.
[14] M. R. Tarasevich, B. N. Efremov, in *Electrodes of Conductive Metallic Oxides Part A* (Ed: S. Trasatti), Elsevier, New York **1982**, p. 227.
[15] C. Z. Yuan, L. Yang, L. R. Hou, J. Y. Li, Y. X. Sun, X. G. Zhang, L. F. Shen, X. J. Lu, S. L. Xiong, X. W. Lou, *Adv. Funct. Mater.* **2012**, *22*, 2560..
[16] J. B. Wu, Y. Lin, X. H. Xia, J. Y. Xu, Q. Y. Shi, *Electrochim. Acta* **2011**, *56*, 7163.
[17] C. Z. Yuan, L. Yang, L. R. Hou, L. F. Shen, X. G. Zhang, X. W. Lou, *Energy Environ. Sci.* **2012**, DOI:10.1039/c2ee21745g.
[18] H. S. Zhou, D. L. Li, M. Hibino, I. Honma, *Angew. Chem. Int. Ed.* **2005**, *44*, 797.
[19] C. C. Hu, K. H. Chang, M. C. Lin, Y. T. Wu, *Nano Lett.* **2006**, *6*, 2690.
[20] D. N. Futaba, K. Hata, T. Yamada, T. Hiraoka, Y. Hayamizu, Y. Kakudate, O. Tanaike, H. Hatori, M. Yumura, S. Iijima, *Nat. Mater.* **2006**, *5*, 987.
[21] B. Cui, H. Lin, Y. Z. Liu, J. B. Li, P. Sun, X. C. Zhao, C. J. Liu, *J. Phys. Chem. C* **2009**, *113*, 14083.
[22] T. Choudhury, S. O. Saied, J. L. Sullivan, A. M. Abbot, *J. Phys. D: Appl. Phys.* **1989**, *22*, 1185.
[23] J. F. Marco, J. R. Gancedo, M. Gracia, *J. Solid State Chem.* **2000**, *153*, 74.
[24] Y. E. Roginskaya, O. V. Morozova, E. N. Lubnin, Y. E. Ulitina, G. V. Lopukhova, S. Trasatti, *Langmuir* **1997**, *13*, 4621.
[25] V. M. Jimenez, A. Fernandez, J. P. Espinos, A. R. Gonzalez-Elipe, *J. Electron Spectrosc. Relat. Phenom.* **1995**, *71*, 61.
[26] T. Choudhury, S. O. Saied, J. L. Sullivan, A. M. Abbot, *J. Phys. D: Appl. Phys.* **1989**, *22*, 1185.
[27] J. G. Kim, D. L. Pugmire, D. Battaglia, M. A. Langell, *Appl. Surf. Sci.* **2000**, *165*, 70.
[28] J. H. Zhong, A. L. Wang, G. R. Li, J. W. Wang, Y. N. Ou, Y. X. Tong, *J. Mater. Chem.* **2012**, *22*, 5656.
[29] Y. Wang, C. X. Guo, J. H. Liu, T. Chen, H. B. Yang, C. M. Li, *Dalton Trans.* **2011**, *40*, 6388.